UDK 678.7:66.017
Professional article/Strokovni članek

ISSN 1580-2949
MTAEC9, 46(6)695(2012)

THE EFFECTS OF MICRO AND NANO $CaCO_3$ ON THE RHEOLOGICAL AND PHYSICO/MECHANICAL BEHAVIOR OF AN SBS/$CaCO_3$ COMPOSITE

VPLIV MIKRO- IN NANODELCEV $CaCO_3$ NA REOLOŠKO IN FIZIKALNO/MEHANSKO VEDENJE KOMPOZITA SBS/$CaCO_3$

Mohsen Sadeghi[1], Amirhossein Esfandiari[2]

[1]Department of Polymer Engineering, Faculty of Technical and Engineering, Post- Graduate Center, Islamic Azad University, South Tehran Branch, Tehran, I. R. Iran
[2]Department of Textile Engineering, Faculty of Technical and Engineering, Islamic Azad University, South Tehran Branch, Tehran, I. R. Iran
ah_esfandiari@azad.ac.ir, a.h.esfandiari@gmail.com

Prejem rokopisa – received: 2012-04-03; sprejem za objavo – accepted for publication: 2012-08-27

Different particle sizes of $CaCO_3$ were used and this was confirmed with the X-ray diffraction method. The nano $CaCO_3$ was added, from mass fraction (*w*) 1 % to 5 %, in the styrene butadiene styrene elastomer (SBS). Elastomer nanocomposites were compounded on a two-roll mill and molded in a compression-molding machine. The mechanical properties such as the tensile strength, the elongation at fracture, the modulus at 300 % elongation, the hardness, the specific gravity, the swelling index, and the flame retardancy were studied. The results were compared with a commercial $CaCO_3$ (μm) filled SBS. There was an improvement in the properties of the elastomer nanocomposites because of the uniform dispersion of the nano $CaCO_3$ particles in the matrix that intercalates the elastomer chains. Hence, the degree of cross-linking increases multifold in comparison with the commercial $CaCO_3$.

Keywords: swelling index (SI), flame retardancy, vulcanized, dicumil peroxide (DCUP), MFI and nano $CaCO_3$

Uporabljeni so bili delci $CaCO_3$ različne velikosti, potrjeni z metodo rentgenske difrakcije. Elastomeru stiren butadien stiren (SBS) je bilo dodano od 1 % do 5 % masnih deležev (*w*) nanodelcev $CaCO_3$. Nanokompozitni elastomer je bil izdelan z dvovaljčnim mlinom in ulit na tlačnem stroju. Preizkušene so bile mehanske lastnosti, kot so natezna trdnost, raztezek pri porušitvi, modul pri 300-odstotnem raztezku, trdota, specifična gostota, indeks nabrekanja, zadrževanje širjenja plamena. Rezultati so bili primerjani s komercialnim SBS, polnjenim z mikrodelci $CaCO_3$. Ugotovljeno je bilo izboljšanje lastnosti elastomernega kompozita zaradi enakomerne razpršenosti nanodelcev $CaCO_3$ v osnovi, kar omogoča vrinjenje verig elastomera. Zato je mogoča večkratno povečana stopnja prepletanja v primerjavi s komercialnim $CaCO_3$.

Ključne besede: indeks nabrekanja (SI), zadrževanje širjenja plamena, vulkanizirano, dikumil peroksid (DCUP), MFI in nanodelci $CaCO_3$

1 INTRODUCTION

In recent years, combinations of inorganic nanoparticles and polymers have received a great deal of interest[1–6] for the reason that they provide a means of improving the strength together with the toughness of the polymer matrix, which is almost impossible with conventional filled polymers. The performance of the polymer nanocomposites is strongly dependent on the final morphology of the nanoparticles dispersed in the polymer matrix. Various methods[7–10] have been used to prepare polymer nanocomposites, but most of them are complicated and costly[1–4].

The effect of mineral fillers on the elastic modulus of polymers has been widely studied and there are many theoretical models available for predicting the behavior of a composite in the elastic zone[6]. Thermoplastic elastomers are materials that combine the characteristics of the good processing ability of thermoplastics with the physical properties of vulcanized rubber.

The mechanical and thermal properties of polymers and composite structures can be improved through the use of various kinds of fillers. Micron-sized fillers usually cause a decrease in strength, impact resistance, and processability. The application of nanotechnology in elastomer nanocomposites shows a significant improvement in the modulus, strength, toughness, and resistance to chemical attack, gas impermeability in polymer composites[1–5].

In this study, three different sizes of $CaCO_3$ were used as filler in styrene butadiene styrene (SBS) and compared with commercial $CaCO_3$ composites of SBS/$CaCO_3$. The mechanical properties and physical properties were studied and compared with other fillers[6–8]. The effect of mineral fillers on the elastic modulus of polymers has been widely studied and there are many theoretical models available for predicting the behavior of a composite in the elastic zone[9–11]. Thermoplastic rubbers are materials that combine the characteristics of the good process ability of thermoplastics with the physical properties of vulcanized rubber. SEBS is an elastomer that has been subjected to a hydrogenation process, through which the polybutadiene chain is eliminated. This new rubber has a high resistance to environment, temperature, UV radiation, etc[12]. This is without losing the properties of a thermoplastic, so making them

useful in applications where a standard SBS is not useful. SBS is a thermoplastic material that successfully combines the properties of an elastomer (rubber) with the low costs of processing thermoplastics.

2 EXPERIMENTAL PROCEDURE

2.1 Materials

The SBS elastomer used in this study was a commercial TPE grafted with maleic anhydride function, 2600 S-40B supplied from RTP Co., USA. The stearic acid, nano-sized calcium carbonate with an average particle size of 50–70 nm, with a bulk density of 0.4 g/cm^3 and a pH of 9.2 and commercial $CaCO_3$ with a bulk density of 0.81 g/cm^3 and a pH 8.6 was supplied from Omya Co., Austria. The DCUP (Bis (1-methyl-1-phenylethyl) peroxide) for the curing agent was supplied from MERCK Co., Germany.

2.2 Preparation of the composite

At the beginning the nanometer and macrometer (commercial) calcium carbonate particulates were first dried at a temperature of 75 °C for 2 h, then premixed with the SBS elastomer together with different $nCaCO_3$ and $mCaCO_3$ loadings (w = 1–5 %) and with DCP and physically mixed in a mixer with a rotor speed of 75 r/min at 30 °C for 30 min (before the materials for making every master-batch with a 0.1 balance were weighed). This procedure was performed in order to achieve a homogeneous dispersion of nanoparticles. The temperature cannot be more than 30 °C because the DCP may change the solid state to a liquid phase and lead to the aggregation of $CaCO_3$. The resulting master-batch (all the master-batches were 100 g) was then extruded on a Brabender twin-screw extruder at 60 r/min and (140, 160, 180, 200) °C for each sample. The extruder compounds were fed into a compression set mold to make a molded kind of specimen shape for the tensile and other tests (Dumbbell and circular plate) using ASTM standards (D638 and D395).The formulation of the samples is given in **Table 1**.

Table 1: Sample specification
Tabela 1: Specifikacija vzorcev

Sample	SBS	$nCaCO_3$	$\mu CaCO_3$	DCP
Neat (S 1)	99	0	0	1
1 % Nc-HPC (S 2)	97	1	1	1
3 % Nc-HPC (S 3)	93	3	3	1
5 % Nc-HPC (S 4)	89	5	5	1

2.3 Characterization method

Scanning electron microscopy (SEM) was performed with a Tescan 130 VEGA-II apparatus equipped with an energy beam of 20 kV. The prepared samples were cryogenically fractured in liquid nitrogen and then coated with gold by vapor deposition using a vacuum sputtering machine before the SEM observation. Therefore, the SEM images were all obtained by inspecting the cryogenically fractured surfaces of the samples.

The mechanical properties tests were carried out on a TCS-2000 Universal Testing Machine (GOTECH, Taiwan) at a crosshead speed of 500 mm/min and 23 °C according to the ASTM D 412 method, and the stress-strain curves were drawn simultaneously. The hardness tests were carried out with a Durometer Hardness tester (TECLOOCK, Japan) (shore) in accordance with ASTM D 2240 at 23 °C. The MFI test was carried out on a GT-7100-MI (GOTECH, Taiwan) with ASTM D 1234 at 220 °C, 5 kg. The specific gravity carried out per ASTM D792. The shrinkage carried out per ASTM D 955.

3 RESULTS AND DISCUSSION

3.1 Rheological characterization

3.1.1 Isothermal curing behavior

Figure 1 illustrates the rheographic profile of neat SBS, SBS/$nCaCO_3$ and SBS/$\mu CaCO_3$ blends containing mass fractions (1, 3 and 5) % at (140, 160, 180 and 200) °C. From each of the curves shown in **Figure 1**, some characteristic parameters were determined, as listed in **Table 2**. These parameters included T_∞ and T_0 as the maximum and minimum torques during the curing process; the time during which the torque begins to rapidly increase as the onset of the curing and also the whole curing time. It is evident that at a given $nCaCO_3$ loading, an increase in the isothermal curing temperature drives the curing reaction forward, as well as decreasing the curing time. The reason for such an observation could be correlated with the availability of more thermal energy in addition to the lower viscosity of the compound, which facilitates the formation of the cross-linking networks[13]. A closer view of the experimental data showed that $nCaCO_3$ nanoparticles introduced to the system seem to act as accelerators with respect to the curing reaction times. This acceleration effect should be related to the fact that the stearic acid layer on the $nCaCO_3$ surface possesses strong acid sites to activate the electrophiles effectively at the curing temperature[14]. Therefore, it can be inferred that there is a relatively high concentration of curing agents on the surface of the nanofiller at the beginning, which then advances into the unreacted zone in the $nCaCO_3$ modified SEBS blends. Interestingly, it can be observed that the higher the $nCaCO_3$ loading, the shorter the curing time for the SBS systems. In other words, the addition of treated $nCaCO_3$ increases the thickness of the stearic acid layer on the nanofiller surface, which provides extra regimes for the cross-linking reaction; and thus a further catalyzing effect occurs during the curing reaction. However, one cannot ignore the contribution of the large surface area of the $nCaCO_3$ particles, which ensures the proper, sufficient and increased dispersion of the radical reactant. It is well known that

the maximum torque of the rheometer curves is the most relevant factor with respect to the cross-link density of the cured systems[13,14]. The retractive force to resist a deformation is proportional to the number of network-supporting polymer chains per unit of thermoset and the higher number of junctures increases the number of supporting chains[15]. In this regard, T_∞ is expected to increase at a higher value of the network chain density. However, as can be observed in **Table 2**, the variation of the minimum torque concerning the curing temperature and the composition of the sample is not so appreciably related to the maximum torque.

Hence, the difference $T = T_\infty - T_0$ is normally used to analyze the experimental data in order to exclude the effect of T_0. As is clear from the obtained ΔT values, there is a tendency to increase this value as the amount of $nCaCO_3$ content increases up to 3 %. In contrast, dissimilar behavior was observed for the effect of the curing temperature on the torque value. In this case the availability of more thermal energy helps the segmental and diffusional chain motion, which leads to a lower torque value[16,17].

3.1.2 Isothermal cure kinetics

The torquemeter test results under isothermal conditions yielded valuable information about the amount of torque versus time that could be used to evaluate the kinetic parameters by using a series of mathematical expressions. In this concern, the degree of curing, β, which was employed to indicate the extent of the resin cross-linking, might be estimated from the time dependency of the torque values using the following equation[18]:

$$\beta = \frac{T_{(t)} - T_0}{T_\infty - T_0} \tag{1}$$

where $T(t)$ is the torque at a given time of the curing process. There are two primary mechanisms describing most thermoset curing, including the n^{th}-order and the autocatalytic[19]. The n^{th}-order model assumes that the reaction rate is proportional to the concentration of the unreacted material $(1 - \theta)$, as shown in Eq. (2), where n is the reaction order[20]:

$$\frac{d\beta}{dt} = K\,(1 - \theta)^n \tag{2}$$

Nevertheless, the n^{th}-order model seems to be incapable of describing the progress of the entire reaction because several simultaneous reactions may occur during the curing process[21]. For an isothermal reaction, the n^{th}-order mechanism predicts the maximum reaction rate at time = 0. However, this is not the case for autocatalytic curing processes, in which the final products of the curing reaction can catalyze the subsequent reaction between the resin and the hardener. On the other hand, in an autocatalytic model, the conversion rate is proportional to the concentration of both the unreacted and the reacted material:

$$\frac{d\beta}{dt} = K\,(1 - \beta)^n \beta^m \tag{3}$$

where m is also a reaction order. In both the autocatalytic and n^{th}-order models, K represents the temperature-dependent reaction rate constant, obeying the well-known Arrhenius equation as[22]:

$$K = A\,\exp\left(\frac{-E}{RT}\right) \tag{4}$$

where A is a frequency factor corresponding to the incidence of molecular collisions that should be obtained to produce a chemical reaction. In addition, E, R and T are

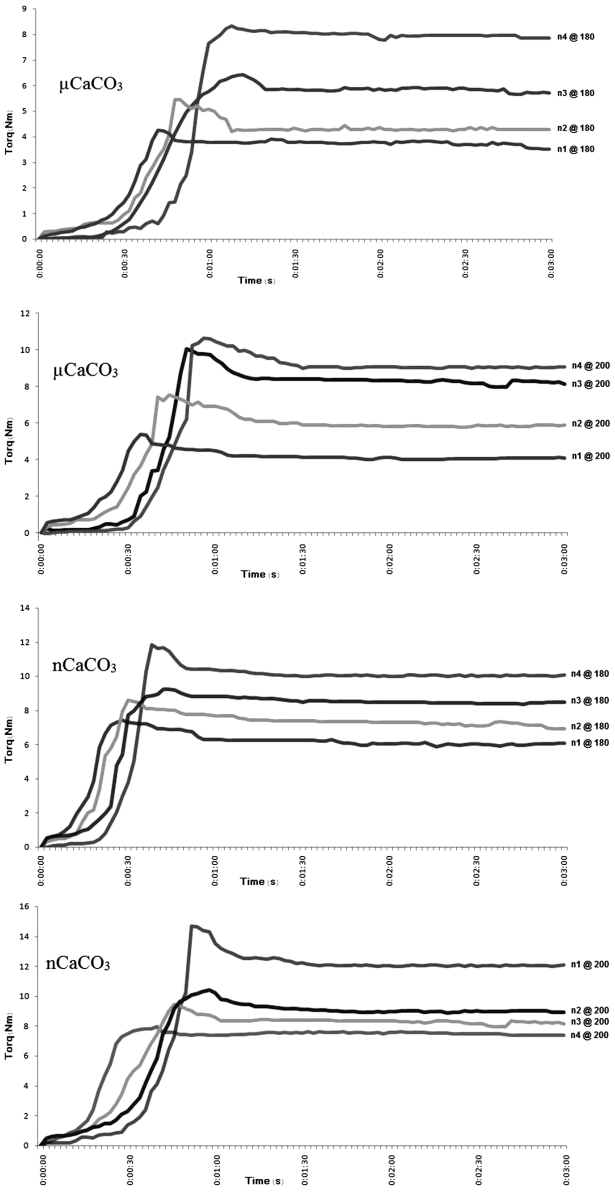

Figure 1: Torque (T) as a function of curing time for neat and filled systems containing 5 % $nCaCO_3$ and μ $CaCO_3$ at the analyzed temperatures

Slika 1: Navor (T) kot funkcija časa do uravnoteženja za čist in polnjen sistem s 5 % nanodelcev $CaCO_3$ in mikrodelcev $CaCO_3$ pri temperaturah preizkušanja

Table 2: T_0 and T_∞ obtained from the rheometer curves for $nCaCO_3$ (**Figure 1**), for all of the samples at the analyzed temperatures
Tabela 2: T_0 in T_∞, dobljena iz rheometrskih krivulj za nanodelce $CaCO_3$ (**slika 1**), za vse vzorce pri temperaturah preizkušanja

Sample	Curing temperature (°C)	T_0/(N m)	T_∞/(N m)	ΔT	Onset of cure (s)	Curing time (s)
Neat	140	0.235	3.83	3.595	23	34
	160	0.315	6.412	6.097	20	36
	180	0.466	6.807	6.341	13	37
	200	0.575	8.845	8.27	10	42
1 % Nc-HPC	140	0.545	6.976	6.431	37	18
	160	0.615	9.215	8.6	29	24
	180	1.126	10.694	9.568	19	42
	200	1.356	12.396	11.04	16	50
3 % Nc-HPC	140	1.075	8.795	7.72	24	30
	160	1.49	12.327	10.837	20	37
	180	1.356	12.741	11.376	16	39
	200	0.854	14.365	13.511	11	44
5 % Nc-HPC	140	0.47	8.236	7.766	19	24
	160	1.045	11.7	10.655	15	26
	180	1.425	12.431	11.006	13	34
	200	0.912	15.883	14.971	10	38

Table 3: T_0 and T_∞ obtained from the rheometer curves for $\mu CaCO_3$ (**Figure 1**), for all of the samples at the analyzed temperatures
Tabela 3: T_0 in T_∞, dobljena iz rheometrskih krivulj za mikrodelce $CaCO_3$ (**slika 1**), za vse vzorce pri temperaturah preizkušanja

Sample	Curing temperature (°C)	T_0/(N m)	T_∞/(N m)	ΔT	Onset of cure (s)	Curing time (s)
Neat	140	0.06	2.67	2.61	26	28
	160	0.27	5.14	4.87	25	30
	180	0.73	6.34	5.61	14	33
	200	0.05	7.19	7.14	13	37
1 % Nc-HPC	140	0.38	4.81	4.43	42	16
	160	0.27	7.16	6.89	32	21
	180	0.09	9.21	9.12	22	36
	200	1	10.91	9.91	18	42
3 % Nc-HPC	140	1.6	7.23	5.63	26	21
	160	2.43	9.85	7.42	24	28
	180	2.29	11.40	9.11	18	34
	200	2.24	12.36	10.12	10	39
5 % Nc-HPC	140	1.24	7.91	6.67	20	23
	160	0.88	9.53	8.65	14	25
	180	1.63	11.84	10.21	11	33
	200	0.28	13.68	13.40	10	38

Table 4: Combination of the curing kinetic model parameters determined from the curve fits of $d\theta/dt$ versus θ and the values of the n^{th}-order and autocatalytic mechanism activation energies for all of the samples at the analyzed temperatures for $nCaCO_3$
Tabela 4: Kombinacija parametrov modela kinetike uravnoteženja, določenih iz krivulj $d\theta/dt$ proti θ in vrednosti n-tega reda ter aktivacijske energije avtokatalitičnega mehanizma za temperature preizkušanja za nanodelce $CaCO_3$

Sample	Curing temperature (°C)	K_1/ ($\times 10^{-4}$ s^{-1})	K_2/ ($\times 10^{-2}$ s^{-1})	m	N	R^2	E_1/ (K J/mol)	E_2/ (K J/mol)
Neat	140	1.23	1.04	1.17	1.23	0.99		
	160	7.03	4.14	1.46	1.26	0.98		
	180	11.15	4.87	1.53	1.32	0.99		
	200	13.05	5.21	1.49	1.54	0.98	15.31	48.79
1 % Nc-HPC	140	1.13	1.18	1.33	0.90	0.98		
	160	6.42	4.26	1.24	1.17	0.99		
	180	11.75	5.49	0.98	1.28	0.99		
	200	13.48	6.18	1.33	1.34	0.98	17.67	53.44
3 % Nc-HPC	140	2.37	2.57	1.29	1.24	0.99		
	160	8.79	6.41	1.67	1.33	0.98		
	180	12.07	8.69	1.74	1.38	0.98		
	200	14.48	9.31	1.69	1.41	0.98	19.21	68.74
5 % Nc-HPC	140	3.51		1.54	1.15	0.99		
	160	8.89		1.33	1.23	0.99		
	180	12.44		0.97	1.35	0.98		
	200	14.56		1.24	1.44	0.99	23.66	89.77

Table 5: Combination of the curing kinetic model parameters determined from the curve fits of $d\theta/dt$ versus θ and the values of the n^{th}-order and the autocatalytic mechanism activation energies for all of the samples at the analyzed temperatures for μ$CaCO_3$

Tabela 5: Kombinacija parametrov modela kinetike uravnoteženja, določenih iz krivulj $d\theta/dt$ proti θ in vrednosti n-tega reda ter aktivacijske energije avtokatalitičnega mehanizma za temperature preizkušanja za mikrodelce $CaCO_3$

Sample	Curing temperature (°C)	K_1 ($\times 10^{-4}$ s^{-1})	K_2 ($\times 10^{-2}$ s^{-1})	m	N	R^2	E_1/ (K J/mol)	E_2/ (K J/mol)
Neat	140	3.42	1.13	1.17	1.23	0.99		
	160	7.12	6.42	1.46	1.26	0.98		
	180	8.85	11.75	1.53	1.32	0.99		
	200	9.76	13.48	1.49	1.54	0.98	14.12	39.24
1 % Nc-HPC	140	1.13	3.51	1.33	0.90	0.98		
	160	6.42	8.89	1.24	1.17	0.99		
	180	11.75	12.44	0.98	1.28	0.99		
	200	13.48	14.56	1.33	1.34	0.98	16.33	47.35
3 % Nc-HPC	140	1.04	1.23	1.29	1.24	0.99		
	160	6.41	7.03	1.67	1.33	0.98		
	180	8.69	11.15	1.74	1.38	0.98		
	200	9.31	13.05	1.69	1.41	0.98	17.42	63.57
5 % Nc-HPC	140	4.26	3.25	1.54	1.15	0.99		
	160	5.49	8.46	1.33	1.23	0.99		
	180	7.18	12.03	0.97	1.35	0.98		
	200	10.57	14.22	1.24	1.44	0.99	21.04	83.66

the activation energy, the gas constant and the absolute temperature, respectively. Commonly, the isothermal curing of the thermoset material may be the result of more than one type of chemical reaction[23]. This combination of reactions can be represented by the generalized expression given by Kamal and Sourour:

$$\frac{d\beta}{dt} = A_1 \exp\left(\frac{-E_1}{RT}\right)(-\theta)^n + A_2 \exp\left(\frac{-E_2}{RT}\right)(1-\theta)^n \theta^m \quad (5)$$

The first term in this model corresponds to an n^{th}-order reaction and the second one is attributed to an autocatalytic reaction occurring during the curing reaction of the material under study[24,25].

All the values were rounded up to two decimal places according to the error bands associated with 95 % confidence limits. A careful inspection of the calculated m and n values reveals that there is no trend for the systematic variation of either m or n with temperature during the isothermal curing of samples with the $nCaCO_3$ loading. As already reported by many authors, this conclusion is expected to be reached theoretically, since m and n do not depend on the curing temperature and the nanofiller content.

In addition, the curing kinetic characterizations (**Tables 2** to **5**) show a direct proportionality between both the n^{th}-order and the autocatalytic reaction-rate constants and also the value of the curing temperature. However, for all the samples, the K_2 value was higher than K_1, which suggests the autocatalytic mechanism was more favorable than the other one. A variety of reasons might be given for the large K_2 value, including the fact that the reaction mixture is very viscous. Indeed, because of the high viscosity, upon completing the initial uncatalyzed reaction, the reactants cannot move away; they would rather sequester together. As a result, they are more prepared for subsequent catalyzed reactions. It is interesting to note that the increment of the $nCaCO_3$ content increases the rate constant obtained for the systems, which seems to be connected with the higher SBS chains absorbed on the stearic treated nanofiller surface rather than the catalytic effect of the $nCaCO_3$. In addition, the value of the n^{th}-order and autocatalytic activation energies (E_1 and E_2) can be determined from the slope of the linear relationship between (K_1) and (K_2) versus $1/T$ (plots not shown here). The numerical values calculated for the above-mentioned parameters are represented in **Table 3** for all of the samples. Interestingly, both E_1 and E_2 are sharply decreased with the increment of the $nCaCO_3$ content. This observation is consistent with the discussion previously mentioned, that the curing rate of SBS systems increases when raising the $nCaCO_3$ content. Consequently, a lower amount of energy for curing, together with a shorter curing time for the $nCaCO_3$-containing SBS samples over the neat blends, could offer the coating's formulators an excellent approach to meeting the requirements of today's challenges in the coating market. The curing results are shown in **Tables 2** and **3**.

3.2 Physical properties

3.2.1 Flame Retardancy (FR) and TGA analyses

The thermal decomposition was verified using 10 mg samples in an aluminum holder under a nitrogen or air flow (50 cm^3 min^{-1}), heated from 25 °C to 600 °C at different heating rates of (5, 10, 20 and 40) °C min^{-1}.

The TGA curves and the differential (DTG) curves were measured with a Shimadzu TGA-50 thermo-

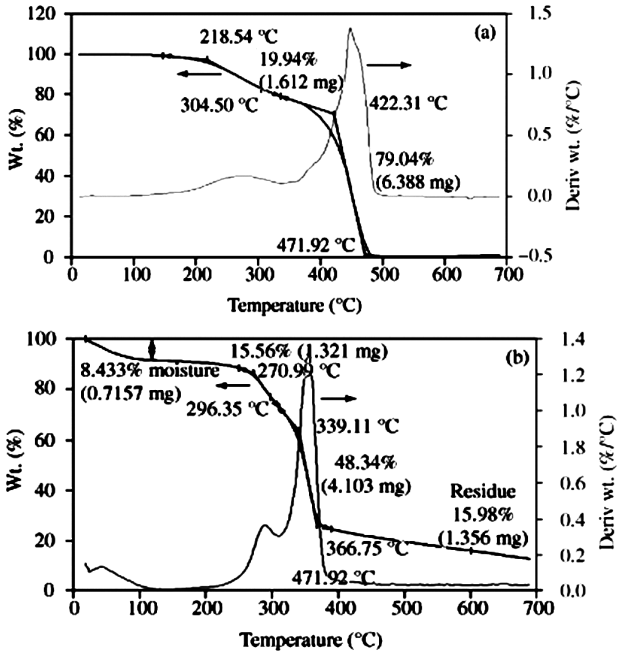

Figure 2: TGA curve for: a) SBS/5 % $nCaCO_3$, b) SBS/5 % $\mu CaCO_3$
Slika 2: TGA-krivulja za: a) SBS/5 % nanodelcev $CaCO_3$, b) SBS/5 % mikrodelcev $CaCO_3$

gravimetric analyzer. The apparent activation energy as a function of the degree of decomposition in air and nitrogen atmospheres was calculated by the Ozawa method[25].

According to **Figures 2a** and **b**, the SBS thermal profile was not affected by the $nCaCO_3$ addition. In **Figure 1b**, the TGA curves show the degradation steps attributed to the components of the $nCaCO_3$. The flammability values were 2.1 s/mm and 1.8 s/mm, respectively, for the 5 % nanosize $CaCO_3$ and the commercial $CaCO_3$. This means a reduction in the nanosize shows a better improvement in the FR. This might be due to the nano filler forming an effective layer on the surface, which absorbs the heat of burning (**Figure 3**).

The FR test was carried out in a flame tester (prolific make), as per ASTM-D 4804. The sample was clamped 85 mm above the horizontal screen so that it would not sag out to touch the screen. The free end is exposed to specify the gas flame for 30 s. The sample was clamped at a 45° angle with the flame trip. The time required for burning and the relative rate of burning were measured.

3.2.2 Swelling Index and MFI

The swelling index (SI), an indirect way of measuring the total cross-link density, which in turn is correlated to the physical properties of the various vulcanized materials was determined by swelling a small piece of sample in the toluene for 24 h at room temperature:

$$SI = \frac{X - Y}{Y} \tag{6}$$

where X = the weight of the sample after swelling and Y = the weight of the sample before swelling.

There is an increment in SI for all the compositions up to 3 % additions of nano and commercial $CaCO_3$ filler; the SI decreases for all cases (**Table 6**). At 5 % of filler loading, the *SI* is 1.43 and 2.44, respectively, for nanometer-size $CaCO_3$ and the commercial $CaCO_3$ filler. The swelling first increases up to 1 % of $CaCO_3$ filled in SBS, and subsequently decreases with an increase in the amount of filler. This is due to greater cross-linking of the SBS, as a uniform dispersion of nano $CaCO_3$ brings the chains closer and keeps them intact with nanoparticles; even if the amount of nano addition is less. The MFI test for each sample in **Figure 4** shows that the effect of the nano size $CaCO_3$ filler has a better curing effect on the SBS matrix, because with a decrease of MFI, the matrix curing is high.

Table 6: Swelling Index for $nCaCO_3$ and $\mu CaCO_3$
Tabela 6: Indeks nabrekanja nanodelcev $CaCO_3$ in mikrodelcev $CaCO_3$

sample	kind	Initial mass (g)	Swollen mass (g)	Swelling Index
Neat		5	8.8	1.76
5 % Nc-HPC (Mic)	Nano	5	7.7	1.54
	Micron	5	12.55	2.51
5 % Nc-HPC (Nano)	Nano	5	7.15	1.43
	Micron	5	12.15	2.44

The swelling indexes of two kinds of $CaCO_3$ composite are shown in **Table 6**. The results show that with an

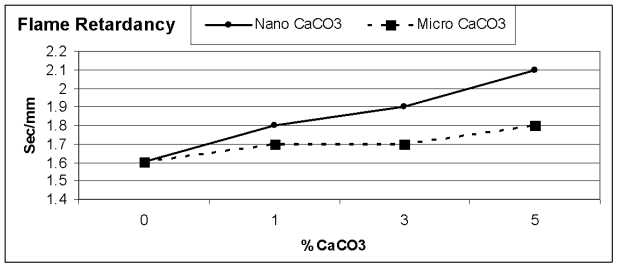

Figure 3: Flame retardancy comparison between the micro and nano samples
Slika 3: Primerjava zadrževanja plamena med mikro- in nanovzorci

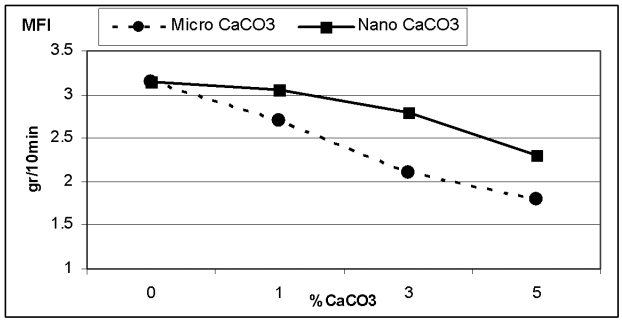

Figure 4: MFI Comparison between $nCaCO_3$/SBS and $\mu CaCO_3$/SBS
Slika 4: MFI-primerjava med nanodelci $CaCO_3$/SBS in mikrodelci $CaCO_3$/SBS

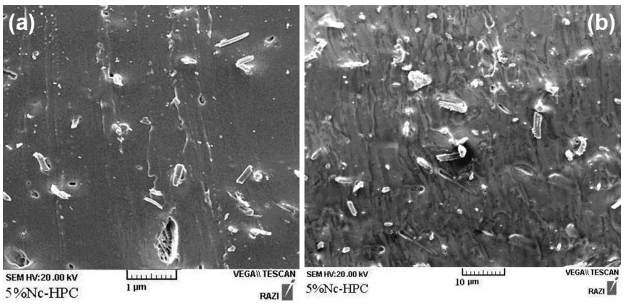

Figure 5: Scanning electronic micrographs for: a) 5 % $nCaCO_3$, b) SBS/5 % $\mu CaCO_3$

Slika 5: SEM-posnetek: a) 5 % nanodelcev $CaCO_3$, b) SBS/5 % mikrodelcev $CaCO_3$

increase of mass fractions w(%) nano $CaCO_3$, rather than the w(%) micro $CaCO_3$, the swelling index is decreased. The decrease in the hardness with the reduction in the nano size is due to a greater and uniform dispersion of filler in the matrix, which brings the chains of the matrix closer to reduce the free volume to a greater extent in the cross-linking of chains.

3.3 Morphological characterization

The SEM micrographs, as shown in **Figure 5**, revealed that the nanoparticles were reasonably well dispersed in the SBS systems with 5 % $nCaCO_3$ and $\mu CaCO_3$ loadings after the processing and dispersion steps.

3.4 Mechanical properties

3.4.1 Tensile properties

The tensile strength of the composites with a small particle size is higher than that of the others (**Figure 6**).

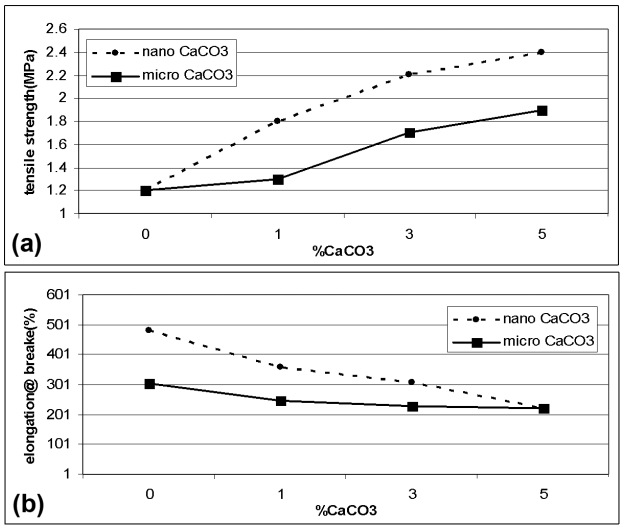

Figure 6: Mechanical properties comparison between $nCaCO_3$/SBS and $\mu CaCO_3$/SBS: a) tensile strength, b) elongation at break

Slika 6: Primerjava mehanskih lastnosti med nanodelci $CaCO_3$/SBS in mikrodelci $CaCO_3$/SBS: a) natezna trdnost, b) raztezek pri porušitvi

The tensile strength of 5 % nano $CaCO_3$ (**Figure 7**) filled SBS (2.4 MPa for $nCaCO_3$) is higher than the commercial $CaCO_3$ (1.9 MPa for $\mu CaCO_3$). This means that the nano $CaCO_3$ provides a higher tensile strength than the commercial $CaCO_3$ filled SBS. This increment in tensile strength is due to the uniform dispersion of nano filler into the elastomer matrix that intercalates the elastomer matrix, and hence the degree of cross-linking of the elastomer chains increases. The elongation at the break decreases by an increase of mass fraction w(%) $CaCO_3$, for which this parameter in $\mu CaCO_3$ is clearer than the nano size. This decrement is such that the degree of cross-linking of the elastomer chains increases.

3.4.2 Specific Gravity and Hardness

The compression-molded specimens were tested to provide hardness data by using a shore-A hardness tester, as per ASTM D 2240. An analytical balance equipped with a stationary support for an immersion vessel above or below the balance pan was used for the specific gravity measurement, as per ASTM D 792. The corrosion-resistant wire for suspending the specimen and the sinker for an analytical balance equipped with a stationary support for an immersion vessel above or below the balance pan was used for the specific gravity measurement, as per ASTM D 792. A corrosion-resistant wire for suspending the specimen and a sinker for the lighter specimen (specific gravity < 1) were employed. A beaker was used as an immersion vessel, a test specimen of convenient size was weighed in air, and then the specimen was suspended from a fine wire attached to a balance and completely immersed in distilled water. The weight of the specimen in water was determined (with a sinker):

$$Specific\ gravity = \frac{a}{(a+w)-b} \tag{7}$$

where a is the weight of the specimen in air, b is the weight of the specimen (with a sinker) and the wire in

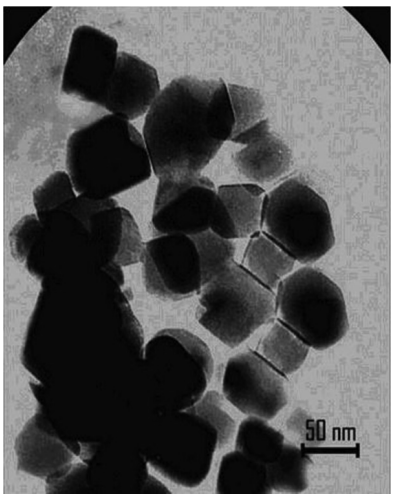

Figure 7: TEM image of as-received $CaCO_3$ nanoparticles

Slika 7: TEM-posnetek nanodelcev $CaCO_3$ v dobavljenem stanju

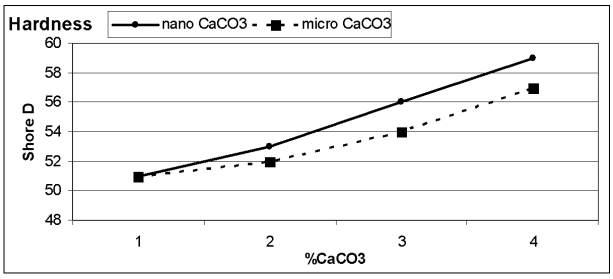

Figure 8: Hardness comparison between the nano $CaCO_3$ sample and the micro $CaCO_3$ sample
Slika 8: Primerjava trdote vzorcev nanodelcev $CaCO_3$ in mikrodelcev $CaCO_3$

water, *w* is in this equation the weight of the totally immersed sinker and the partially immersed wire.

There is a continuous increment in the specific gravity for all the compositions in comparison to the pure SBS (**Table 7**). The increment in the specific gravity is more appreciable in the case of the nanometer $CaCO_3$ (0.959 at 5 %) than for the commercial $CaCO_3$ (0.948 at 5 %).

Table 7: Specific gravity testing
Tabela 7: Specifična gostota

sample	Specific gravity $nCaCO_3$, (g/cm^3)	Specific gravity $\mu CaCO_3$, (g/cm^3)
Neat	0.930	0.930
1 % Nc-HPC	0.943	0.936
3 % Nc-HPC	0.952	0.943
5 % Nc-HPC	0.959	0.948

The hardness of all the compositions increases with an increase in the amount of filler (0–5 %) in the case of the nano and commercial $CaCO_3$ (**Figure 8**). The nanometer $CaCO_3$ shows a higher value of the hardness than the commercial of $CaCO_3$. The increase in the specific gravity and the hardness with a reduction in the nano size is due to a greater and more uniform dispersion of filler in the matrix, which brings the chains of matrix closer to reduce the free volume to a greater extent in the cross-linking of chains.

4 CONCLUSIONS

This study set out to investigate the effect of stearic-acid-coated $CaCO_3$ nanoparticles and commercial $CaCO_3$ on the physical characteristics and morphology, the curing behavior, and the mechanical properties of the SBS elastomer blend. The morphological studies were performed by XRD, TEM and SEM methods, and the results clearly indicated a suitable dispersion of $nCaCO_3$ in the matrix. The nano $CaCO_3$ shows a drastic improvement in the mechanical properties, the swelling index, the specific gravity, and the flame-retardancy indices than the commercial $CaCO_3$-filled SBS. The reduction to the nanosize gives more enhancements in the properties due to a uniform dispersion of nanoparticles into the elastomer matrix that interrelates the elastomer chains and increases the degree of cross-linking of the matrix.

5 REFERENCES

[1] S. Mishra, N. G. Shimpi, Comparison of Nano $CaCO_3$ and flyash filled with styrene butadiene rubber on mechanical thermal properties, Journal of Scientific & Industrial Research, 64 (**2005**), 44–751

[2] M. Eroglu, Effect of Talc and Heat Treatment on the Properties of Polypropylene/EVA Composite, International Journal of Science & Technology, 2 (**2007**) 1, 63–73

[3] F. Sahnoune, J. M. Lopez-Cuesta, A. Crespy, Effect of elastomer interfacial agents on tensile and impact properties of $CaCO_3$ filled HDPE, Journal of Materials Science, 34 (**1999**), 535–544

[4] A. H. Esfandiari, H. Nazokdast, et al., Review of Polymer-Organoclay Nanocomposites, Journal of Applied Sciences, 8 (**2008**) 3, 545–561

[5] A. H. Esfandiari, H. Nazokdast et al., Investigation of Effect of Organoclay and Compatibilizer on Microstructure and Mechanical Properties of PP/PA6/Montmorillonite Nanocomposite, 6th International Conference of Textile Science (TEXSCI 2007), Liberec, Czech Republic, Book of Abstract, 2007, 31–32

[6] S. R. Ahmad, S. Husseinsyah, K. Hussin, The Effects of Chemical Modifiers on the Thermal Properties of Calcium Carbonate Filled Polypropylene/Ethylene Propylene Diene Terpolymer Composites, Pertanika, J. Sci. & Technol., 19 (**2011**) 1, 153–159

[7] A. H. Esfandiari, Characterization and Preparation of Extrusion-Cast HDPE-Clay Nanocomposite, 4th International Textile, Clothing and Design Conference- Magic World of Textiles, Dubrovnik, Croatia, Book of Proceedings, 2008, 69–72

[8] V. Gaulliard, J. L. Leblanc, A Rheometrical Technique to Study the Swelling Kinetics of Vulcanized Rubber Particles by Paraffinic Solvents Using a Torque Rheometer, Journal of Applied Polymer Science, 94 (**2004**), 142–153

[9] L. H. C Mattoso, F. C. Ferreira, A. A. S. Curvelo, Sisal fiber: morphology and applications in polymer composites. In: Proceedings of the International Symposium on Lignocellulosic-Plastics Composites, 1996

[10] A. Zarafshan, S. Zarafshan, A. H. Esfandiari, Analytical Investigation on Efficiency Evaluation of Fibre Reinforced Polymers Confinement on Square Reinforced Concrete Columns, Materiale Plastice, 48 (**2011**) 4, 285–288

[11] A. H. Esfandiari, Mechanical Properties of PP/Jute and Glass Fibers Composites: The Statistical Investigation, Journal of Applied Sciences, (**2007**) 7, 3943–3950

[12] S. Mishra, S. H. Sonawane, R. P. Singh, A. Bendale & K. Patil, Effect of nano Mg (OH) on the mechanical and flame retarding properties of PP composites, J Appl Polym Sci, 94 (**2004**), 116

[13] W. Luo, N. Zhou, Z. Zhang, H. Wu, Effects of vibration force field on structure and properties of HDPE/$CaCO_3$ nanocomposites, Polymer Testing, 25 (**2006**), 124–129

[14] Kusmono, Z. A. Mohd Ishak, W. S. Chow, T. Takeichi, Rochmadi, Influence of SEBS-g-MA on morphology, mechanical, and thermal properties of PA6/PP/organoclay nanocomposites, European Polymer Journal, 44 (**2008**), 1023–1039

[15] S. Mishra, N. G. Shimpi, U. D. Patil, Effect of Nano $CaCO_3$ on thermal properties of Styrene Butadiene Rubber (SBR), J Polym Res, 14 (**2007**), 449–459

[16] S. Mishra, S. H. Sonawane, N. Badgujar, K. Gurav, D. Patil, Comparative study of mechanical and flame retarding properties of polybutadiene rubber filled with nanoparticle and flyash, J Appl Polym Sci, 96 (**2005**), 6

[17] R. Herzig, W. E. Baker, Correlations Between Image Analysed Morphology and Mechanical Properties of Calcium carbonate-Filled PP, Journal of Materials Science, 28 (**1993**), 6531

[18] K. Premphet, P. Horanont, Phase Structure and Property Relationship in Ternary PP/Elastomer/Filler Composites, Journal of Applied Polymer Science, 74 (**1999**), 3445

[19] Z. Bartczak, A. S. Argon, R. E. Cohen, T. Kowalewski, The morphology and orientation of PE in films of sub-micron thickness crystallized in contact with calcite and rubber substrates, Polymer, 40 (**1999**), 2367

[20] B. Pukanszky, F. Tudos, J. Jancar, J. Kolarik, The Possible Mechanisms of Polymer-Filler Interaction in PP/$CaCO_3$ Composites, Journal of Material Science Letters, 8 (**1989**), 1040

[21] A. Khare, A. Mitra, Effect of $CaCO_3$ on the Crystallization Behavior of PP, Journal of Material Science, 31 (**1996**), 569

[22] Y. C. Lee, R. S. Porter, Cavitation during Isothermal Crystallization of Isotactic Polypropylene, Polymer Engineering Science, 26 (**1986**), 633

[23] S. Mishra, S. H. Sonawane, R. P. Singh, Studies on characterization of nano $CaCO_3$ prepared by in-situ deposition technique and its applications in PP-nano $CaCO_3$ composites, J Polym Sci Part B: Polym Phys, 43 (**2005**), 107

[24] A. L. F. de Moura Giraldi, R. Cardoso de Jesus, R. Mei, L. H. Innocentini, The influence of extrusion variables on the interfacial adhesion and mechanical properties of recycled PET composites, Journal of Materials Processing Technology, 162–163 (**2005**), 90

[25] C. H. Lee, H. B. Kim, S. T. Lim, H. S. Kim, Y. K. Kwon, H. J. Choi, Ordering behavior of layered silicate nanocomposites with a cylindrical triblock copolymer, Macromol Chem Phys., 207 (**2006**) 4, 444–55